Science
AAAS

# Supplementary Materials for

## Quantum control of trapped polyatomic molecules for eEDM searches

Loïc Anderegg *et al*.

Corresponding authors: Loïc Anderegg, anderegg@g.harvard.edu; Nicholas R. Hutzler, hutzler@caltech.edu

*Science* **382**, 665 (2023)
DOI: 10.1126/science.adg8155

**The PDF file includes:**

## ZERO $g$-FACTOR STATES

### Origin

In $^2\Sigma$ electronic states of linear polyatomic molecules, the spin-rotation interaction, $\gamma\vec{N}\cdot\vec{S}$, couples the molecular rotation $N$ and the electron spin $S$ to form the total angular momentum $J$. These states are well described in the Hund's case (b) coupled basis. An applied electric field $E_Z$ will interact with the molecular-frame electric dipole moment $\mu_E$, connecting states with opposite parity, $\Delta M_F = 0$, and $\Delta J \leq 1$. When $\mu_E E_Z \gg \gamma$, $N$ and $S$ are uncoupled and well described by their lab frame projections $M_N$ and $M_S$. However, in the intermediate field regime with $\mu_E E_Z \sim \gamma$, the molecular eigenstates are mixed in both the Hund's case (b) coupled basis and the decoupled basis. $M_F$ remains a good quantum number in the absence of transverse fields. In this regime, $M_F \neq 0$ states with $\langle M_S\rangle = 0$ can arise at specific field values. These states have no first order electron spin magnetic sensitivity, and, unlike $M_F = 0$ clock states, have large eEDM sensitivity near $B_Z = 0$. We refer to these states as *zero g-factor* states [6].

Zero $g$-factor states arise from avoided level crossings as free field states are mixed by the electric field. One of the crossing states has $\langle M_S\rangle < 0$, the other state has $\langle M_S\rangle > 0$, and both have mixed $M_N$. The spin-rotation interaction couples the states and lifts the crossing degeneracy, resulting in eigenstates that are superpositions of electron spin up and down with $\langle M_S\rangle = 0$, while retaining non-zero molecular orientation with $\langle\hat{n}\rangle = \langle M_N\ell\rangle \neq 0$. The lab frame projection of $\hat{n}$ ensures that the eEDM interaction in the molecule frame does not rotationally average away.

Zero $g$-factor states are generically present in the Stark tuning of polyatomic molecules. The reduction of symmetry in a polyatomic molecule allows for rotation about the internuclear axis, resulting in closely spaced doublets of opposite parity. When these doublets are mixed by an applied electric field, they split into $2N+1$ groups of levels representing the values of the molecular orientation $\langle M_N\ell\rangle$. For each $N$ manifold with parity doubling, avoided level crossings generically occur between an $M_N\ell = \pm 1$ Stark manifold and an $M_N\ell = 0$ Stark manifold.

In diatomic molecules without parity-doubling, the existence of zero $g$-factor states requires an inverted spin rotation structure ($\gamma < 0$), such that the two $J$ states are tuned closer to each other by an electric field. For example, the YbF molecule ($\gamma = -13.4$ MHz [39, 40]) has zero $g$-factor states at $E \approx 866$ V/cm in the $N = 1$ manifold, while CaF does not. However, since $|\gamma|/B \ll 1$ for most $^2\Sigma$ diatomic molecules, the electric fields that mix spin-rotation states are much less than those that polarize the molecule. Therefore, zero $g$-factor states occur when the molecule has negligible lab-frame polarization, limiting eEDM sensitivity. For example, the aforementioned states in YbF have $|\langle\Sigma\rangle| \approx 0.006$, which is $\sim$3% the value of $\Sigma$ in the zero $g$-factor states used in this work.

### Characterization

To locate zero $g$-factor crossings and calculate eEDM sensitivities, we model the $\widetilde{X}(010)$ level structure using an effective Hamiltonian approach [41–43]:

$$H_{\text{eff}} = H_{\text{Rot}} + H_{\text{SR}} + H_\ell + H_{\text{Hyp}} + H_{\text{Zeeman}} + H_{\text{Stark}} + H_{\text{ODT}} \tag{S1a}$$

$$H_{\text{Rot}} = B\left(\vec{N}^2 - \ell^2\right) \tag{S1b}$$

$$H_{\text{SR}} = \gamma\left(\vec{N}\cdot\vec{S} - N_z S_z\right) \tag{S1c}$$

$$H_\ell = -q_\ell\left(N_+^2 e^{-i2\phi} + N_-^2 e^{i2\phi}\right) \tag{S1d}$$

$$H_{\text{Hyp}} = b_F\vec{I}\cdot\vec{S} + \frac{c}{3}\left(3I_z S_z - \vec{I}\cdot\vec{S}\right) \tag{S1e}$$

$$H_{\text{Zeeman}} = g_S\mu_B B_Z S_Z \tag{S1f}$$

$$H_{\text{Stark}} = -\mu_Z E_Z \tag{S1g}$$

$$H_{\text{ODT}} = -\vec{d}\cdot\vec{E}_{\text{ODT}} \tag{S1h}$$

Here, we use a similar Hamilton as Ref. [7]. $H_{\text{Rot}}$ is the rotational energy; $H_{\text{SR}}$ is the spin-rotation interaction accurate for low-$N$ bending mode levels, with $z$ defined in the molecule frame; $H_\ell$ is the $\ell$-type doubling Hamiltonian, with $\pm$ defined in the molecule frame, $\phi$ as the nuclear bending coordinate, and using the same phase convention as Ref. [44]; $H_{\text{Hyp}}$ is the hyperfine Fermi-contact and dipolar spin interactions, defined in the molecule frame; $H_{\text{Zeeman}}$

describes the interaction of the electron spin magnetic moment with the lab-frame magnetic field; $H_{\rm Stark}$ is the interaction of the $Z$-component of molecule-frame electric dipole moment $\mu_E$ with the lab frame DC electric field, $E_Z$; and $H_{\rm ODT}$ is the interaction of the molecular dipole moment operator $\vec{d}$ with the electric field of the ODT laser, $\vec{E}_{\rm ODT} = \mathcal{E}_0/2(\hat{\epsilon}_{\rm ODT}e^{-i\omega t} + \text{c.c.})$.

To evaluate the molecule frame matrix elements, we follow the techniques outlined in Refs. [41, 42] to transform into the lab frame. The field-free Hamiltonian parameters are taken from Ref. [46], except for the hyperfine parameters, which were determined by the observed line positions to be $b_F = 2.45$ MHz and $c = 2.6$ MHz, similar to those of the $\widetilde{X}(000)$ state [47]. We use the same dipole moment, $|\mu| = 1.47$ D, as the $\widetilde{X}(000)$ state, determined in Ref. [48]. Matrix elements of $H_{\rm ODT}$ are calculated following Ref. [49] using the 1064nm dynamic polarizabilities reported in Ref. [15].

For the calculations discussed below and in the main text, the ODT is polarized along the laboratory $Z$ axis and the molecules sit at a fixed trap depth of 160 $\mu$K (corresponding to the average trap intensity seen by the molecules in the experiment). As detailed in the main text, when the trapping light is aligned with $E_Z$, it acts like a weak electric field, shifting the zero $g$-factor crossing by $\sim 1$ V/cm from the field-free value. If the trapping light polarization is rotated relative to $E_Z$, tensor light shifts can couple states with $\Delta M_F = \pm 2$ or $\pm 1$ (the linearity of the light ensures there are no $\Delta M_F = \pm 1$ vector shifts) [49]. The effects of this coupling are similar to those of transverse magnetic fields, which we discuss below.

In the current work, we ignore nuclear and rotational Zeeman effects. Specifically, the magnetic sensitivity of CaOH receives small contributions from nuclear spin of the H atom and the rotational magnetic moment of both the electrons and the nuclear framework. While they have not yet been fully characterized, all of these effects will contribute at the $10^{-3}\mu_B$ level or less. These additional $g$-factors do not depend strongly on the applied electric field, and result in a small shift of the zero $g$-factor crossing location. Future work characterizing rotational magnetic moments of $\widetilde{X}(010)$ states of laser-coolable metal hydroxides can enable more accurate predictions of zero $g$-factor field values.

In CaOH, each rotational state $N$ supports multiple $M = \pm 1$ pairs of zero $g$-factor states. The states at finite electric field can be labeled in terms of their adiabatically correlated zero-field quantum numbers $|N, J^p, F, M\rangle$. In the presence of trap shifts, the zero $g$-factor states for $N = 1$ occur at $E = 59.6$ V/cm for $|J = 1/2^+, F = 1, M = \pm 1\rangle$ and at $E = 64.1$ V/cm for $|J = 3/2^+, F = 1, M = \pm 1\rangle$. The $J = 1/2, M = 1$ state is a superposition of 47% $M_N\ell = -1$, 50% $M_N\ell = 0$, and 3% $M_N\ell = 1$, while the $J = 3/2, M = 1$ state is 43% $M_N\ell = -1$, 48% $M_N = 0$, and 9% $M_N\ell = 1$. Both states are weak-electric-field seekers, yet the opposite molecule frame orientation of the spin results in differences in the value of $\Sigma$ and the $g$-factor slope. For CaOH, the magnetic sensitivity and eEDM sensitivity of $N = 1$ zero $g$-factor states are shown in Fig. S1.

By diagonalizing $H_{\rm eff}$ over a grid of $(E_Z, B_Z)$ values, we can obtain 2D plots of $g$-factors and eEDM sensitivities shown in Fig. S2. For generality, we consider the molecular structure in the absence of trap shifts. Using the $Z$-

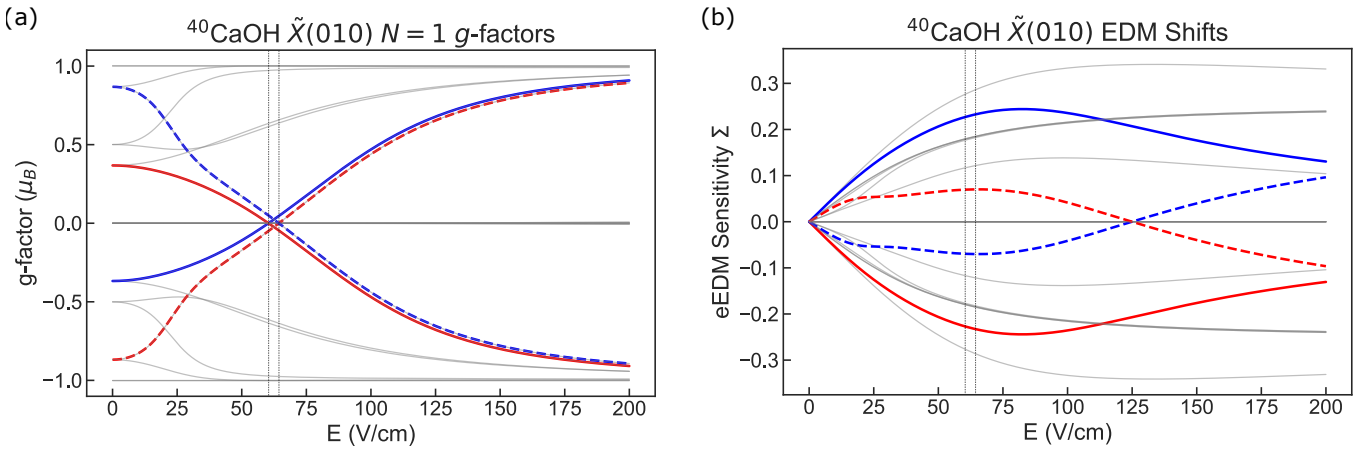


FIG. S1. Electric field tuning of $N = 1$ zero $g$-factor states near $B_Z = 0$ in the absence of trap shifts. Blue lines denote $M_F = +1$ states and red lines $M_F = -1$. Solid traces denote the $J = 1/2$ state pair and dashed traces denote the $J = 3/2$ pair. The dotted vertical lines mark the electric field value of the zero $g$-factor crossing without trap shifts, ≈60.5 V/cm for $J = 1/2$ and ≈64.4 V/cm for $J = 3/2$. Grayed out traces are other states in the $N = 1$ manifold. (a) The $g$-factor $g_S\mu_B\langle M_S\rangle$ as a function of the applied electric field. (b) eEDM sensitivity $\langle\Sigma\rangle$ as a function of the applied electric field. A consequence of the Hund's case (b) coupling scheme is that $\Sigma$ asymptotes to a maximum magnitude of $S/(N(N+1)) = 1/4$ for fields where the parity doublets are fully mixed but rotational mixing is negligible [45]. For fields where $J$ is not fully mixed, some states can exhibit $|\Sigma| > 1/4$.

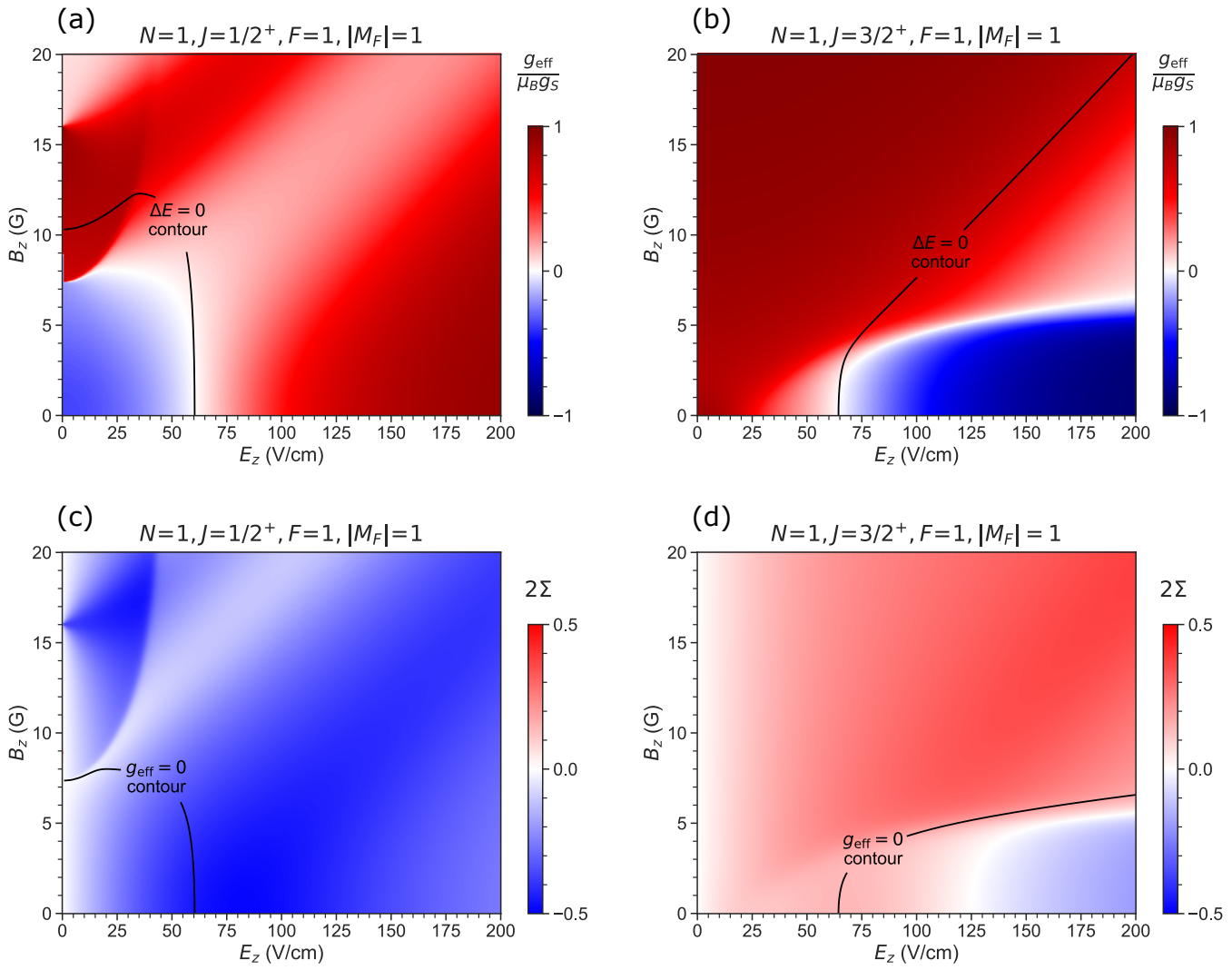


FIG. S2. Full electric and magnetic characterization of zero $g$-factor states in the $N = 1$ manifold of CaOH, without trap shifts. (a, b) 2D plots of the effective $g$-factor difference between two $M = \pm 1$ states, defined by $g_{\text{eff}} = g_S \mu_B (\langle M_S \rangle_{M=+1} - \langle M_S \rangle_{M=-1})$. The plotted $g$-factor is normalized by $g_S \mu_B$. The black line represents the contour where the $M = \pm 1$ levels are nominally degenerate. (c, d) 2D plots of the eEDM sensitivity, $\langle \Sigma \rangle_{M=+1} - \langle \Sigma \rangle_{M=-1}$. The black line represents the $g_{\text{eff}} = 0$ contour.

symmetry of the Hamiltonian, we separately diagonalize each $M_F$ block to avoid degeneracies at $B_Z = 0$. Continuous 2D surfaces for eigenvalues and eigenvectors are obtained by ordering eigenstates at each value of $(E, B)$ according to their adiabatically correlated free field state. The application of an external magnetic field parallel to the electric field results in $\langle M_S \rangle \neq 0$ for an individual zero $g$-factor state, but the differential value between a zero $g$-factor pair can still have $\Delta \langle M_S \rangle = 0$. This differential value means the superposition of a zero $g$-factor pair can maintain magnetic insensitivity and EDM sensitivity over a range of fields, for example up to $\sim$5 G for the $J = 1/2, N = 1$ pair.

The procedure we use here for identifying zero $g$-factor states can be generically extended to searching for favorable transitions between states with differing eEDM sensitivities, similar to what has been already demonstrated in a recent proposal to search for ultra-light dark matter using SrOH [7]. In addition, there are also fields of $B_Z \approx 10 - 20$ G and $E_Z \approx 0$ where opposite parity states are tuned to near degeneracy. This is the field regime that has been proposed for precision measurements of parity-violation in optically trapped polyatomic molecules [9].

We note that zero $g$-factor pairs also occur in $N = 2^-$. The crossings occur around $400 - 500$ V/cm for states correlated with the negative parity manifold. Since many interactions increase in magnitude with larger $N$, the overall electric field scale of the intermediate regime increases. Additionally, the robustness of zero $g$-factor states also improves, with some pairs able to maintain $\Delta \langle M_S \rangle = 0$ for magnetic fields up to 40 G. These $N = 2$ pairs also have non-zero eEDM sensitivity for a wide range of magnetic field values.

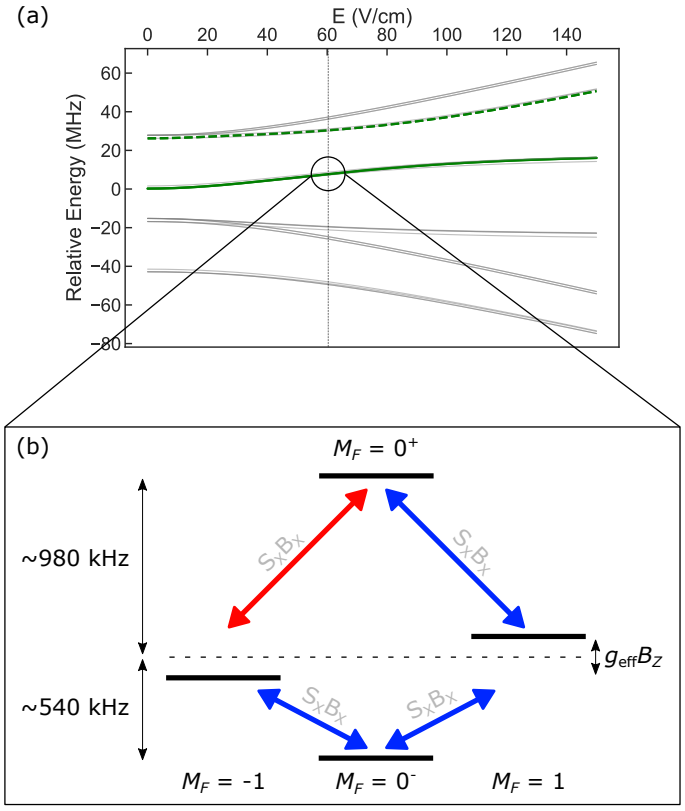


FIG. S3. (a) Stark shifts for $N = 1$ in CaOH. The $J = 1/2^+$ zero $g$-factor states are shown with a solid green line, while the $J = 3/2^+$ zero $g$-factor states are indicated with a dashed green line. All other levels are grayed out. A vertical dotted line indicates the location of the $J = 1/2^+$ zero $g$-factor crossing. (b) A zoomed in level diagram of the $J = 1/2^+$ zero $g$-factor hyperfine manifold. The bias field splitting $g_{\text{eff}} B_Z$ is not to scale. Transverse field couplings are shown with double sided arrows, with blue (red) indicating negative (positive) $S_X$ matrix element.

## TRANSVERSE MAGNETIC FIELDS

### Transverse Field Sensitivity

We now expand our discussion to include the effect of transverse magnetic fields. Their effects can by modeled by adding $B_X S_X$ and $B_Y S_Y$ terms to the effective Hamiltonian, which have the selection rule $\Delta M_F = \pm 1$. For this discussion, we focus on the level structure of the $N = 1, J = 1/2^+$ manifold in CaOH near the zero $g$-factor crossing at 60.5 V/cm in the absence of trap shifts, shown in Figure S3. We note if there were no nuclear spin $I$, the two zero $g$-factor states would be $M_J = \pm 1/2$ states separated by $\Delta M = 1$. In such a case these degenerate states would be directly sensitive to transverse fields at first order, thereby reducing the $g$-factor suppression.

Due to the hyperfine structure from the nuclear spin of the H atom in CaOH, the degenerate $M_F = \pm 1$ states in a zero $g$-factor pair are coupled by second order transverse field interactions. These interactions are mediated via the $M_F = 0^\pm$ states, where $\pm$ denotes the upper or lower states. Using a Schrieffer–Wolff (aka Van-Vleck) transformation, we can express the effective Hamiltonian matrix for second order coupling between the $M_F = \pm 1$ states. We write the states as $|M_F\rangle$, and for convenience we take the transverse field to point along $X$:

$$H_{+1,-1} = -(g_S \mu_B B_X)^2 \left( \frac{\langle -1|S_X|0^+\rangle \langle 0^+|S_X|+1\rangle}{\Delta E_{0^+}} + \frac{\langle -1|S_X|0^-\rangle \langle 0^-|S_X|+1\rangle}{\Delta E_{0^-}} \right) \tag{S2}$$

Here, $\Delta E_{0^\pm}$ is the energy difference of the $M_F = 0^\pm$ levels from the $M_F = \pm 1$ levels. Our model provides the following values: $\langle 0^-|S_X|+1\rangle = \langle 0^-|S_X|-1\rangle = -0.18$, $\langle 0^+|S_X|+1\rangle = -0.16$, and $\langle 0^+|S_X|-1\rangle = 0.16$. The difference in sign is a result of Clebsh-Gordon coefficient phases, and only the relative phase is relevant. We also have $\Delta E_{0^+} = 0.98$ MHz and $\Delta E_{0^-} = -0.54$ MHz. The combination of phases precludes the possibility of destructive interference. With these

parameters and defining $g_\perp = H_{+1,-1}/B_X$, then eqn. S2 evaluates to $(g_S\mu_B B_X)^2(0.086/\text{MHz}) \approx (0.68\ \text{MHz/G}^2)B_X^2$. Our model estimates the transverse sensitivity at $B_X \sim 1$ mG to be $g_\perp\mu_B \sim 7\times10^{-4}$ MHz/G, of the same order as the neglected nuclear and rotational Zeeman terms. The suppressed transverse field sensitivity bounds the magnitude of $B_Z$, which must be large enough to define a quantization axis for the spin, $g_{\text{eff}}B_Z \gg g_\perp B_\perp$.

### Cancellation of transverse magnetic fields

When transverse magnetic fields are dominant, the electron will be quantized along the transverse axis and there is minimal spin precession by the bias $B_Z$ field. The transverse coupling results in eigenstates given by $(|M_F = 1\rangle \pm e^{i\phi}|M_F = -1\rangle)/\sqrt{2}$, where the phase $\phi$ is set by the direction of $\vec{B}$ in the transverse plane. If $\phi = 0$ or $\pi$, only one of these states is bright to the $\hat{X}$-polarized state preparation microwaves, which means the initial state is stationary under the transverse fields. For all other orientations, the transverse field causes spin precession with varying contrast, depending on the specific value of $\phi$.

We are able to use transverse spin precesion to measure and zero transverse fields to the mG level. We do so by operating with minimal bias field $B_Z \approx 0$ and operating $E_Z$ near the zero $g$-factor crossing, such that $g_{\text{eff}}B_Z < g_\perp B_\perp$. We then apply a small transverse magnetic field to perform transverse spin precession. Here, the dynamics are dominated by the transverse fields rather than the $Z$ fields. We obtain field zeros by iteratively minimizing the precession frequency by tuning the bias fields $B_X$ and $B_Y$.

## IMPERFECT FIELD REVERSAL

We briefly present a systematic effect involving non-reversing fields in eEDM measurements with zero $g$-factor states and discuss methods for its mitigation. The electric field dependence of $g_{\text{eff}}$ can mimic an eEDM signal when combined with other systematic effects, very much like in $^3\Delta_1$ molecules [25, 26]. When the sign of $E_Z$ is switched, a non-reversing electric field $E_{\text{NR}}$ will cause a $g$-factor difference of $g_{\text{NR}} = (\mathrm{d}g_{\text{eff}}/\mathrm{d}E_Z)E_{\text{NR}}$. This will give an additional spin precession signal $g_{\text{NR}}B_Z$. By perfectly reversing $B_Z$ as well, this precession signal can be distinguished from a true EDM signal. However, if there is also a non-reversing magnetic field $B_{\text{NR}}$, there will still be a residual EDM signal given by $(\mathrm{d}g/\mathrm{d}E)E_{\text{NR}}B_{\text{NR}}$. Using the measured slope of ∼0.03 (MHz/G)/(V/cm), and using conservative estimates of $E_{\text{NR}} \sim 1$ mV/cm and $B_{\text{NR}} \sim 1$ $\mu$G, we obtain an estimate precession frequency of ∼30 $\mu$Hz. While this is an order of magnitude smaller than the statistical error for the current best eEDM measurement measurement [50], it is still desirable to devise methods to reduce the effect further.

Performing eEDM measurements at different zero $g$-factor states can help suppress systematic errors resulting from the above mechanism. For example, the $N = 1, J = 3/2$ zero crossing has a different magnitude for $\Sigma$, which can be used to distinguish a true eEDM from a systematic effect. Both $N = 1$ crossings are only separated by ∼4 V/cm. Furthermore, the zero $g$-factor states in $N = 2^-$ can also be used for systematic checks, as they additionally offer different $g_{\text{eff}}$ vs $E_Z$ slopes as well as different $\Sigma$ values. The $N = 2^-$ states can be populated directly by the photon-cycling used to pump into the bending mode.

## SPIN PRECESSION NEAR ZERO *G*-FACTOR

As discussed in the main text, the longest achievable coherence times occur at at combination of low effective $g$-factors (which suppress $\delta B_Z$ decoherence) and low magnetic bias fields (which suppress $\delta\mu_{\text{eff}}$ decoherence). These low $g$-factors and bias fields only very weakly enforce a quantization axis along $Z$, enhancing the potential for transverse magnetic fields $B_\perp$ to contribute. Such fields have the effect of (a) reducing the spin precession contrast and (b) altering the observed precession frequency. To avoid these effects, the condition $g_{\text{eff}}B_Z > g_\perp B_\perp$ must therefore be satisfied. To achieve this, we zero the transverse magnetic fields by intentionally taking spin precession data at $B_Z \approx 0$ and $g_{\text{eff}} \approx 0$ while varying the transverse fields $B_X$ and $B_Y$. By minimizing the spin precession frequency as a function of the transverse fields, we reduce $B_\perp$ to approximately 1 mG. In addition, long-term drifts in the dc magnetic field along all three axes are compensated by actively feeding back on the magnetic field as measured with a fluxgate magnetometer. Under these conditions, at an electric field of 60.3 V/cm (corresponding to $\mu_{\text{eff}} = 0.02$ MHz/G) and a bias field of $B_Z \approx 2$ mG, we achieve a coherence time of 30 ms (Fig. S4).

At these very low bias fields, the molecules are also sensitive to 60 Hz magnetic field noise present in the unshielded apparatus, whose amplitude is on the same order as $B_Z$. Since the experiment is phase stable with respect to the AC

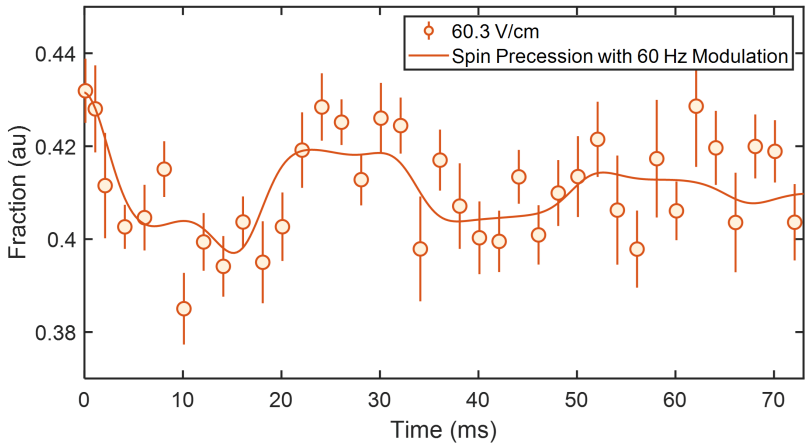


FIG. S4. Spin precession at $E_Z = 60.3$ V/cm and $B_Z = 2$ mG. The fit includes a 60 Hz time-varying magnetic field whose amplitude and phase are measured with a magnetometer. The coherence time fits to 30 ms.

line frequency, this 60 Hz magnetic field fluctuation causes a time-dependent spin precession frequency. A fluxgate magnetometer is used to measure the amplitude and phase of this 60 Hz field, which are then used as fixed parameters in the fit shown in Figure S4.

**References and Notes**


1. M. L. Wall, K. Maeda, L. D. Carr, Simulating quantum magnets with symmetric top molecules. *Ann. Phys.* **525**, 845–865 (2013). doi:10.1002/andp.201300105

2. M. Wall, K. Maeda, L. D. Carr, Realizing unconventional quantum magnetism with symmetric top molecules. *New J. Phys.* **17**, 025001 (2015). doi:10.1088/1367-2630/17/2/025001

3. Q. Wei, S. Kais, B. Friedrich, D. Herschbach, Entanglement of polar symmetric top molecules as candidate qubits. *J. Chem. Phys.* **135**, 154102 (2011). doi:10.1063/1.3649949 Medline

4. P. Yu, L. W. Cheuk, I. Kozyryev, J. M. Doyle, A scalable quantum computing platform using symmetric-top molecules. *New J. Phys.* **21**, 093049 (2019). doi:10.1088/1367-2630/ab428d

5. L. D. Augustovičová, J. L. Bohn, Ultracold collisions of polyatomic molecules: CaOH. *New J. Phys.* **21**, 103022 (2019). doi:10.1088/1367-2630/ab4720

6. I. Kozyryev, N. R. Hutzler, Precision measurement of time-reversal symmetry violation with laser-cooled polyatomic molecules. *Phys. Rev. Lett.* **119**, 133002 (2017). doi:10.1103/PhysRevLett.119.133002 Medline

7. I. Kozyryev, Z. Lasner, J. M. Doyle, Enhanced sensitivity to ultralight bosonic dark matter in the spectra of the linear radical SrOH. *Phys. Rev. A* **103**, 043313 (2021). doi:10.1103/PhysRevA.103.043313

8. N. R. Hutzler, Polyatomic molecules as quantum sensors for fundamental physics. *Quantum Sci. Technol.* **5**, 044011 (2020). doi:10.1088/2058-9565/abb9c5

9. E. B. Norrgard, D. S. Barker, S. Eckel, J. A. Fedchak, N. N. Klimov, J. Scherschligt, Nuclear-spin dependent parity violation in optically trapped polyatomic molecules. *Commun. Phys.* **2**, 77 (2019). doi:10.1038/s42005-019-0181-1

10. Y. Hao, P. Navrátil, E. B. Norrgard, M. Iliaš, E. Eliav, R. G. E. Timmermans, V. V. Flambaum, A. Borschevsky, Nuclear spin-dependent parity-violating effects in light polyatomic molecules. *Phys. Rev. A* **102**, 052828 (2020). doi:10.1103/PhysRevA.102.052828

11. I. Kozyryev, L. Baum, K. Matsuda, B. L. Augenbraun, L. Anderegg, A. P. Sedlack, J. M. Doyle, Sisyphus laser cooling of a polyatomic molecule. *Phys. Rev. Lett.* **118**, 173201 (2017). doi:10.1103/PhysRevLett.118.173201 Medline

12. B. L. Augenbraun, Z. D. Lasner, A. Frenett, H. Sawaoka, C. Miller, T. C. Steimle, J. M. Doyle, Laser-cooled polyatomic molecules for improved electron electric dipole moment searches. *New J. Phys.* **22**, 022003 (2020). doi:10.1088/1367-2630/ab687b

13. D. Mitra, N. B. Vilas, C. Hallas, L. Anderegg, B. L. Augenbraun, L. Baum, C. Miller, S. Raval, J. M. Doyle, Direct laser cooling of a symmetric top molecule. *Science* **369**, 1366–1369 (2020). doi:10.1126/science.abc5357 Medline

14. N. B. Vilas, C. Hallas, L. Anderegg, P. Robichaud, A. Winnicki, D. Mitra, J. M. Doyle, Magneto-optical trapping and sub-Doppler cooling of a polyatomic molecule. *Nature* **606**, 70–74 (2022). doi:10.1038/s41586-022-04620-5 Medline

15. C. Hallas, N. B. Vilas, L. Anderegg, P. Robichaud, A. Winnicki, C. Zhang, L. Cheng, J. M. Doyle, Optical trapping of a polyatomic molecule in an ℓ-type parity doublet state. *Phys. Rev. Lett.* **130**, 153202 (2023). doi:10.1103/PhysRevLett.130.153202 Medline

16. M. Zeppenfeld, B. G. U. Englert, R. Glöckner, A. Prehn, M. Mielenz, C. Sommer, L. D. van Buuren, M. Motsch, G. Rempe, Sisyphus cooling of electrically trapped polyatomic molecules. *Nature* **491**, 570–573 (2012). doi:10.1038/nature11595 Medline

17. A. Prehn, M. Ibrügger, R. Glöckner, G. Rempe, M. Zeppenfeld, Optoelectrical cooling of polar molecules to submillikelvin temperatures. *Phys. Rev. Lett.* **116**, 063005 (2016). doi:10.1103/PhysRevLett.116.063005 Medline

18. D. DeMille, J. M. Doyle, A. O. Sushkov, Probing the frontiers of particle physics with tabletop-scale experiments. *Science* **357**, 990–994 (2017). doi:10.1126/science.aal3003 Medline

19. T. E. Chupp, P. Fierlinger, M. J. Ramsey-Musolf, J. T. Singh, Electric dipole moments of atoms, molecules, nuclei, and particles. *Rev. Mod. Phys.* **91**, 015001 (2019). doi:10.1103/RevModPhys.91.015001

20. M. S. Safronova, D. Budker, D. DeMille, D. F. J. Kimball, A. Derevianko, C. W. Clark, Search for new physics with atoms and molecules. *Rev. Mod. Phys.* **90**, 025008 (2018). doi:10.1103/RevModPhys.90.025008

21. C. Cesarotti, Q. Lu, Y. Nakai, A. Parikh, M. Reece, Interpreting the electron EDM constraint. *J. High Energy Phys.* **2019**, 59 (2019). doi:10.1007/JHEP05(2019)059

22. M. Pospelov, A. Ritz, Electric dipole moments as probes of new physics. *Ann. Phys.* **318**, 119–169 (2005). doi:10.1016/j.aop.2005.04.002

23. J. J. Hudson, D. M. Kara, I. J. Smallman, B. E. Sauer, M. R. Tarbutt, E. A. Hinds, Improved measurement of the shape of the electron. *Nature* **473**, 493–496 (2011). doi:10.1038/nature10104 Medline

24. J. Baron, W. C. Campbell, D. DeMille, J. M. Doyle, G. Gabrielse, Y. V. Gurevich, P. W. Hess, N. R. Hutzler, E. Kirilov, I. Kozyryev, B. R. O'Leary, C. D. Panda, M. F. Parsons, E. S. Petrik, B. Spaun, A. C. Vutha, A. D. West; ACME Collaboration, Order of magnitude smaller limit on the electric dipole moment of the electron. *Science* **343**, 269–272 (2014). doi:10.1126/science.1248213 Medline

25. ACME Collaboration, Improved limit on the electric dipole moment of the electron. *Nature* **562**, 355–360 (2018). doi:10.1038/s41586-018-0599-8 Medline

26. W. B. Cairncross, D. N. Gresh, M. Grau, K. C. Cossel, T. S. Roussy, Y. Ni, Y. Zhou, J. Ye, E. A. Cornell, Precision measurement of the electron's electric dipole moment using trapped molecular ions. *Phys. Rev. Lett.* **119**, 153001 (2017). doi:10.1103/PhysRevLett.119.153001 Medline

27. T. S. Roussy, L. Caldwell, T. Wright, W. B. Cairncross, Y. Shagam, K. B. Ng, N. Schlossberger, S. Y. Park, A. Wang, J. Ye, E. A. Cornell, An improved bound on the electron's electric dipole moment. *Science* **381**, 46–50 (2023). doi:10.1126/science.adg4084 Medline

28. R. Alarcon *et al*., Electric dipole moments and the search for new physics. arXiv:2203.08103 [hep-ph] (2022).

29. Y. Zhou, Y. Shagam, W. B. Cairncross, K. B. Ng, T. S. Roussy, T. Grogan, K. Boyce, A. Vigil, M. Pettine, T. Zelevinsky, J. Ye, E. A. Cornell, Second-scale coherence measured at the quantum projection noise limit with hundreds of molecular ions. *Phys. Rev. Lett.* **124**, 053201 (2020). doi:10.1103/PhysRevLett.124.053201 Medline

30. K. Gaul, R. Berger, Ab initio study of parity and time-reversal violation in laser-coolable triatomic molecules. *Phys. Rev. A* **101**, 012508 (2020). doi:10.1103/PhysRevA.101.012508

31. T. A. Isaev, A. V. Zaitsevskii, E. Eliav, Laser-coolable polyatomic molecules with heavy nuclei. *J. Phys. At. Mol. Opt. Phys.* **50**, 225101 (2017). doi:10.1088/1361-6455/aa8f34

32. T. A. Isaev, R. Berger, Polyatomic candidates for cooling of molecules with lasers from simple theoretical concepts. *Phys. Rev. Lett.* **116**, 063006 (2016). doi:10.1103/PhysRevLett.116.063006 Medline

33. I. Kozyryev, L. Baum, K. Matsuda, J. M. Doyle, Proposal for laser cooling of complex polyatomic molecules. *ChemPhysChem* **17**, 3641–3648 (2016). doi:10.1002/cphc.201601051 Medline

34. See supplementary materials.

35. B. L. Augenbraun, J. M. Doyle, T. Zelevinsky, I. Kozyryev, Molecular asymmetry and optical cycling: Laser cooling asymmetric top molecules. *Phys. Rev. X* **10**, 031022 (2020). doi:10.1103/PhysRevX.10.031022

36. B. L. Augenbraun, Z. D. Lasner, A. Frenett, H. Sawaoka, A. T. Le, J. M. Doyle, T. C. Steimle, Observation and laser spectroscopy of ytterbium monomethoxide, $YbOCH_3$. *Phys. Rev. A* **103**, 022814 (2021). doi:10.1103/PhysRevA.103.022814

37. A. Jadbabaie, Y. Takahashi, N. H. Pilgram, C. J. Conn, Y. Zeng, C. Zhang, N. R. Hutzler, Characterizing the fundamental bending vibration of a linear polyatomic molecule for symmetry violation searches. *New J. Phys.* **25**, 073014 (2022). doi:10.1088/1367-2630/ace471

38. L. Anderegg, N. B. Vilas, C. Hallas, P. Robichaud, A. Jadbabaie, J. M. Doyle, N. R. Hutzler, Data for quantum control of trapped polyatomic molecules for eEDM searches. Zenodo (2023); https://doi.org/10.5281/zenodo.8384389.

39. B. E. Sauer, J. Wang, E. A. Hinds, Laser-rf double resonance spectroscopy of $^{174}$YbF in the $X^2\Sigma^+$ state: Spin-rotation, hyperfine interactions, and the electric dipole moment. *J. Chem. Phys.* **105**, 7412–7420 (1996). doi:10.1063/1.472569

40. C. S. Dickinson, J. A. Coxon, N. R. Walker, M. C. L. Gerry, Fourier transform microwave spectroscopy of the $^2\Sigma^+$ ground states of YbX (X=F, Cl, Br): Characterization of hyperfine effects and determination of the molecular geometries. *J. Chem. Phys.* **115**, 6979–6989 (2001). doi:10.1063/1.1404146

41. A. Petrov, A. Zakharova, Sensitivity of the YbOH molecule to PT-odd effects in an external electric field. *Phys. Rev. A* **105**, L050801 (2022). doi:10.1103/PhysRevA.105.L050801

42. J. M. Brown, A. Carrington, *Rotational Spectroscopy of Diatomic Molecules* (Cambridge Univ. Press, 2003).

43. E. Hirota, *High-Resolution Spectroscopy of Transient Molecules*, vol. 40 of Springer Series in Chemical Physics (Springer, 1985).

44. A. Merer, J. Allegretti, Rotational energies of linear polyatomic molecules in vibrationally degenerate levels of electronic $^2\Sigma$ and $^3\Sigma$ states. *Can. J. Phys.* **49**, 2859–2869 (1971). doi:10.1139/p71-343

45. J. M. Brown, The rotational dependence of the Renner-Teller interaction: A new term in the effective Hamiltonian for linear triatomic molecules in Π electronic states. *Mol. Phys.* **101**, 3419–3426 (2003). doi:10.1080/00268970310001645864

46. M. Li, J. A. Coxon, High-resolution analysis of the fundamental bending vibrations in the $\tilde{A}\,^2\Pi$ and $\tilde{X}\,^2\Sigma^+$ states of CaOH and CaOD: Deperturbation of Renner–Teller, spin–orbit and *K*-type resonance interactions. *J. Chem. Phys.* **102**, 2663–2674 (1995). doi:10.1063/1.468643

47. C. Scurlock, D. Fletcher, T. Steimle, Hyperfine structure in the (0,0,0) $\tilde{X}^2\Sigma^+$ state of CaOH observed by pump/probe microwave-optical double resonance. *J. Mol. Spectrosc.* **159**, 350–356 (1993). doi:10.1006/jmsp.1993.1133

48. T. Steimle, D. Fletcher, K. Jung, C. Scurlock, A supersonic molecular beam optical Stark study of CaOH and SrOH. *J. Chem. Phys.* **96**, 2556–2564 (1992). doi:10.1063/1.462007

49. L. Caldwell, M. R. Tarbutt, Sideband cooling of molecules in optical traps. *Phys. Rev. Res.* **2**, 013251 (2020). doi:10.1103/PhysRevResearch.2.013251

50. Z. Lasner, thesis, Yale University (2019).